Proceedings of the 2018 IEEE/ASME International
Conference on Advanced Intelligent Mechatronics (AIM),
Auckland, New Zealand, July 9-12, 2018

High-resolution 3D optical sensing and real-time 3D video data streaming*

Tyler Bell[1,2] and Song Zhang[2]

Abstract— **The first part of this paper discusses the high-resolution, real-time 3D optical sensing techniques that we developed in the optics community. Such technologies could benefit the advanced intelligent mechatronics community as another sensing tool. The second part of this paper discusses our recent development on 3D sensing data compression and streaming that could open new opportunities for the mechatronics community. Our 3D optical sensing technique is based on the digital fringe projection (DFP) method that has merits of speed, resolution, and accuracy, as well flexibility when comparing with other 3D optical imaging methods. Our novel compression method drastically reduces data sizes, and through seamless integration with our 3D sensing system, allows for real-time high-quality 3D data delivery across standard wired and wireless networks. This paper introduces the basic principles of each technology and casts our perspectives on possible applications that our technologies could enable for the mechatronics community.**

I. INTRODUCTION

Advances in two-dimensional (2D) optical sensing and machine/computer vision have provided integrated smart sensing systems for numerous applications [14]. By adding one more dimension, advanced three-dimensional (3D) optical sensing and vision technologies can have much greater impact to scientific researches (e.g., mechatronics, medicine, computer sciences) and industrial practices (e.g., manufacturing, intelligent robotics).

Due to the increased computational power available on personal computers, mobile devices, and in cloud computing, high-speed and high-accuracy 3D sensing techniques have been increasingly sought after by scientists in fields such as biomedical engineering and computer science, by engineers from various industries including manufacturing and entertainment, and even by ordinary people with different technical backgrounds [25]. The availability of consumer-level real-time 3D sensing technologies (e.g., Microsoft Kinect, Intel RealSense, Apple iPhone X) further drives the developments and applications of 3D optical sensing technologies.

3D optical sensing methods can be broadly classified into two categories: passive and active methods. Passive techniques require no active illumination for 3D sensing, and one of the most popular passive methods used in the mechatronics community is based on stereo vision principles [5, 13]. The stereo-vision technique determines depth information by capturing images from at least two different perspectives, finding the corresponding points which are similar between those images, and then by utilizing the calibrated camera parameters and the triangulation relationship between image pairs. Despite its simple system setup, low cost, and rapid image acquisition, stereo vision is not extensively used in applications where high sensing accuracy is required. This is primarily because such a method requires determining corresponding points from a pair of images, and it is fundamentally difficult to achieve high accuracy if an object does not present rich surface texture.

Active methods eliminate the fundamental limitation of the stereo method by actively illuminating the object with pre-known information. For example, the time of light (TOF) technique actively emits modulated light in the time domain and collects the modulated light scattered back by the object. Depth information can then be calculated by determining the time delay from the time that the signal left the device until the signal returned to the device [7]. Since the TOF method does not require triangulation for 3D sensing, its footprint can be small, making it applicable for long range 3D sensing and mobile sensing. For example, the light detection and ranging (LIDAR) technology is based on TOF for long range sensing, and Microsoft Kinect II employs the TOF for mobile applications. However, the achieved depth resolution for TOF systems may not be high as, due to the extremely high traveling speed of light, it is difficult to measure time delays accurately.

The structured light method, another of the active methods, reconstructs 3D information by replacing one of the cameras within a stereo vision system with a projection device, such that structured pattern(s) can be actively projected for correspondence establishment [19]. The projection device can be a fixed pattern projector (such as those used in Apple iPhone X or Microsoft Kinect), or a programmable and flexible digital video projector. Due to the flexibility of digital video projectors, different types of structured patterns can be used, such as random patterns [8], binary structured patterns [19], multi-gray level patterns [18], as well as sinusoidal patterns [23]. Compared with all of the different types of patterns, using the sinusoidal structured patterns, especially combined with phase-shifting algorithms, is overwhelmingly advantageous [21]. The sinusoidal structured patterns are often referred to as *fringe patterns* in the optics community, and the structured light method which uses digital fringe patterns for 3D optical sensing is often

*This work was supported by National Science Foundation under the grant numbers IIS-1637961

[1] Tyler Bell is a graduate student with School of Electrical and Computer Engineering, Purdue University, 465 Northwestern Ave, West Lafayette, IN 47907, United States bell143@purdue.edu

[2] Song Zhang is with Faculty of School of Mechanical Engineering, Purdue University, 585 Purdue Mall, West Lafayette, IN 47907, United States szhang15@purdue.edu

978-1-5386-1854-7/18/$31.00 ©2018 IEEE

called *digital fringe projection (or DFP)*.

Leveraging the unique projection mechanism of single-chip digital-light-processing (DLP) technologies, Zhang and Huang [26] developed what was probably the first-ever, high-speed 3D optical sensing system that achieved 3D shape acquisition, reconstruction, and display at an unprecedented 40 Hz with over 250,000 measurement points per frame. Following this endeavor, numerous real-time techniques including [10, 15, 20, 28] have been developed for 3D shape measurement, leveraging both advanced hardware technologies (e.g., GPU) and new innovations on software algorithms.

The size of 3D data is typically a magnitude larger than that of its 2D counterpart. Therefore, compressing 3D data has emerged as an important issue to be dealt with for large size data storage and visualization. Conventional 3D data representation formats (e.g., STL, OBJ) are effective and generic, yet they usually store (x, y, z) coordinates for each vertex, the connectivity information between vertices, and often surface normal information thus utilizing a lot of storage space. Given our knowledge and experience on 3D optical sensing system development, we developed a sequence of 3D compression techniques for 3D structured light sensors [2–4, 11, 17, 22] that convert 3D data into standard 2D image formats such that the 2D images can be further compressed using mature 2D image compression methods. Sequences of 2D images can also be further compressed using 2D video compression techniques such as using H.264 codec [12].

Recently, Bell et al. [1] developed a novel platform, dubbed *Holostream*, which enables high-quality 3D video communications across existing standard wireless networks and existing mobile hardware devices (e.g., iPhones and iPads). Such a platform advances the quality and capabilities of applications already utilizing real-time 3D data delivery (e.g., teleconferencing, telepresence), and could also enable applications where real-time delivery of high-resolution, high-accuracy 3D video data is especially critical, such as robot-robot and human-robot interactions.

This paper explains the basic principles behind real-time 3D optical sensing using DFP in addition to real-time 3D video compression and streaming techniques. Experimental data will be presented to demonstrate the performance of each technology.

II. PRINCIPLE

This section briefly discusses the principles of real-time 3D optical sensing using a phase-shifting method, as well as real-time 3D video compression and streaming techniques.

A. Real-time 3D sensing using digital fringe projection (DFP) techniques

Figure 1 shows the schematic diagram of a DFP system for 3D optical sensing using the triangulation approach. Using this figure, we can see that Point A on the imaging unit, Point C on the projection unit, and Point B on the object surface form a triangle; such a triangular relationship can be used for 3D reconstruction when the calibration parameters of the camera and the projector are known. The projected pattern contains stripes that vary sinusoidally in one direction, and thus each varying line on the projector can encode unique information. To find the corresponding point C on the projection device for a given camera image point A, epipolar geometry is often used [23].

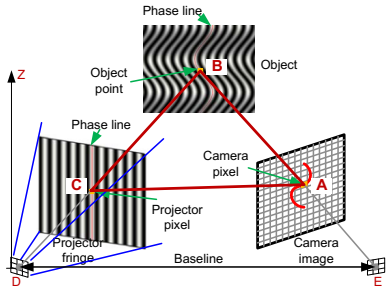

Fig. 1. Schematic configuration of the structured light system. A projector shines pre-defined structured patterns to the object surface; the object surface geometry distorts the patterns; the camera captures the distorted patterns; and the software analyzes the camera images to find their correspondence with the projector in order to form triangulation for 3D reconstruction.

Phase-shifting methods have been extensively employed in high-accuracy 3D optical metrology due to the advantages of achievable speed, resolution, and accuracy [16]. Among those phase-shifting algorithms, the three-step or four-step phase-shifting algorithm is typically used for high-speed applications. For a three-step phase-shifting algorithm with equal phase shifts, the intensity of the three fringe images can be described as

$$I_1(x,y) = I'(x,y) + I''(x,y)\cos(\phi - 2\pi/3), \quad (1)$$
$$I_2(x,y) = I'(x,y) + I''(x,y)\cos(\phi), \quad (2)$$
$$I_3(x,y) = I'(x,y) + I''(x,y)\cos(\phi + 2\pi/3). \quad (3)$$

Here, $I'(x,y)$ is the average intensity, $I''(x,y)$ is the intensity modulation, and $\phi(x,y)$ is the phase to be solved for. Simultaneously solving Eq. (1)-(3), the phase can be obtained via

$$\phi(x,y) = \tan^{-1}\left[\sqrt{3}(I_1 - I_3)/(2I_2 - I_1 - I_3)\right]. \quad (4)$$

Equation (4) provides phase values ranging from $-\pi$ to $+\pi$ with 2π phase discontinuities. A phase unwrapping algorithm is required to determine those 2π discontinuous locations and remove them. In general, phase unwrapping can be classified as either relative phase unwrapping or absolute phase unwrapping. The former produces an unwrapped phase map that can be used to measure relative 3D surface information. Conventional spatial phase unwrapping algorithms [6] typically belong to this category. In contrast, by using a predefined absolute reference, absolute phase unwrapping methods [24] can obtain an unwrapped phase map that can be used to recover absolute 3D shape of the object. Temporal phase unwrapping algorithms typically generate absolute phase maps, for example. In this research, we employ the enhanced two-frequency temporal phase unwrapping method [9] to obtain absolute phase for absolute 3D shape measurement.

In addition to phase, solving Eq. (1)-(3) can also produce a texture image which is perfectly aligned with 3D geometry via

$$I_t(x,y) = \frac{I_1 + I_2 + I_3}{3}. \quad (5)$$

Since the texture image is essentially a regular photograph of the object it can readily be used for enhanced visualizations or for information analysis.

Figure 2 shows an example of using the three-step phase-shifting algorithm for 3D optical sensing. Figures 2(a)-2(c) show three high-frequency fringe patterns. Using these three phase-shifted fringe patterns, we can compute the wrapped phase (Fig. 2(d)) and the raw texture (Fig. 2(k)). Figures 2(e)-2(g) show three low-frequency fringe patterns, from which the low-frequency phase can be calculated, as shown in Fig. 2(h). The low-frequency phase map can be used to unwrap the high-frequency phase map using the enhance two-frequency phase unwrapping method [9]. Figure 2(i) shows the unwrapped phase map. The unwrapped phase map can then be further processed to reconstruct 3D information using the system's calibration parameters. Figure 2(j) shows the 3D result rendered in shaded mode. The raw texture shown in Fig. 2(k) is Bayer coded, which can be converted to color texture using a demosaicing algorithm; Fig. 2(l) shows the recovered color texture. In this example, the system was calibrated using the method discussed in Reference [27]. The camera resolution used for this experiment was 480×640: a rather low resolution, yet the details are well captured by using the phase-shifting method.

Zhang and Huang [26] developed a 3D optical imaging system that simultaneously captured, processed, and displayed 3D geometries at 40 Hz with over 250,000 measurement points per frame, something which was unprecedented at that time. The basic principle behind such a real-time 3D imaging technology is to take advantage of the unique projection mechanism of a single-chip digital light processing (DLP) projector. Such projectors naturally switch between three images (i.e., red, green, and blue channels) at a default refresh rate (which was 80 Hz at that time). Today, the aforementioned enhanced two-frequency phase-shifting algorithm has been successfully implemented on DLP development kits to achieve real-time 3D measurement speeds of 30 Hz (or faster when utilizing a modern GPU to perform the 3D data processing and reconstruction).

B. 3D sensing data compression

Raw 3D video data is enormously large before compression, requiring bandwidths of over 1 Gbps (Gigabit per second) for streaming, which is difficult to achieve across standard wireless networks. To address this, we have developed a two-stage 3D video compression technique which frame-by-frame (1) encodes 3D geometry and color texture into standard 2D images and (2) further compresses the 2D image sequence using standard 2D video compression codecs.

As mentioned above, our 3D sensing technique recovers 3D data from a 2D phase map and, since this process is performed pixel-by-pixel, there exists a one-to-one mapping between the unwrapped phase $\Phi(i,j)$ of a point and its recovered (x,y,z) coordinate. In other words, the 2D phase map already contains a precise encoding of the 3D coordinates. Therefore, as long as the 2D phase map can be encoded, its 3D information can be recovered later on.

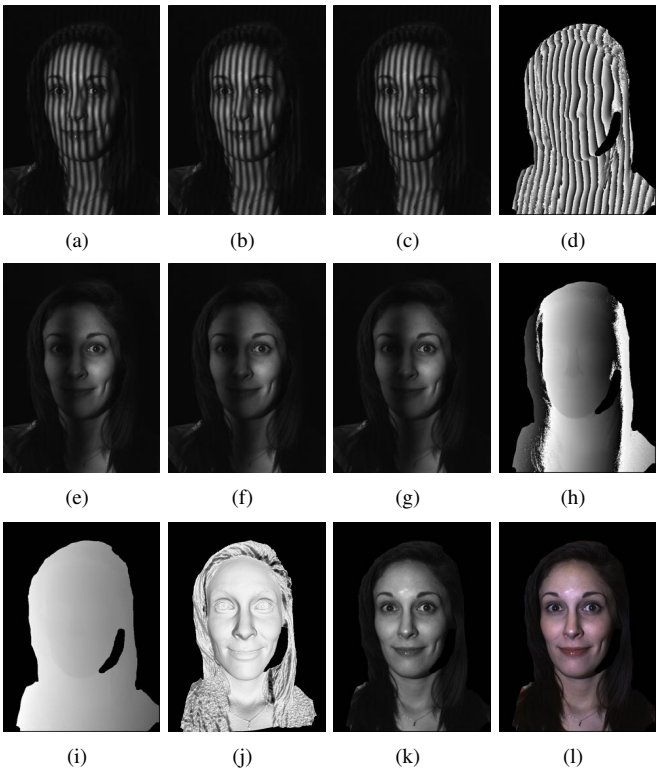

Fig. 2. Example of using enhanced two-frequency phase-shifting method for high-resolution 3D optical sensing. (a)-(c) Three phase-shifted high-frequency fringe patterns; (d) wrapped high-frequency phase map; (e)-(g) three phase-shifted low-frequency fringe patterns; (h) wrapped low-frequency phase map; (i) recovered 3D shape; (k) raw Bayer-coded texture image; (l) color texture after demosaicing. The camera resolution used for this experiment is 480×640.

For each pixel (i,j) within the unwrapped phase map, a scaled corresponding phase value $\widetilde{\Phi}$ is encoded as sine and cosine functions,

$$R(i,j) = 127.5 + 127.5 \sin \widetilde{\Phi}, \quad (6)$$

$$G(i,j) = 127.5 + 127.5 \cos \widetilde{\Phi}, \quad (7)$$

and these two images can be stored into the red and green channels of a standard image. The blue channel is then used to store the natural texture value, $B = I_t$. The encoded 2D image can be further compressed frame by frame via a lossless (e.g., PNG), or via a lossy (e.g., JPEG), image encoding method. The final compressed 2D image can now be stored or transmitted and used to recover both 3D coordinates and color texture when needed.

The left image of Fig. 3 shows an example of an image that encodes both the 3D geometry shown in Fig. 2(j) and color texture shown in Fig. 2(l). If the 480×640 image is stored with lossless PNG, the file size of the data is reduced

from 32 MB to 288 KB, achieving a compression ratio of approximately 112:1 versus storing the same information within the OBJ format. As shown in the last image of Fig. 3(d), the difference between the original geometry and the geometry reconstructed from the PNG image appears to be random noise which may be caused by small amounts of quantization.

(a) (b) (c) (d)

Fig. 3. Encoding and decoding 3D geometry and color texture. A lossless PNG format results in a compression ratio of approximately 112:1. (a) The encoded RGB PNG image; (b) the recovered color texture; (c) the recovered 3D geometry; (d) an overlay of the reconstructed 3D geometry on top of the original 3D geometry (gray color represents recovered geometry and red represents the original geometry).

The encoded RGB image can be further compressed using a lossy JPEG encoder. For example, we can achieve compression ratios of 107:1, 267:1, 406:1, and 518:1 when using JPEG 100%, 95%, 90%, and 85%, respectively. Figure 4 shows the result of compressing one single 3D frame using the different qualities of JPEG encoding. The 3D reconstructions from the lossy encoded images incur some reduction in measurement accuracy; however, for visual-based applications (e.g., telepresence), there may not be a distinguishable difference.

Even higher compression ratios can be achieved if a sequence of encoded 2D frames are compressed using video codecs (e.g., H.264). Figure 5 shows some example reconstructions decoded from the data stored with various qualities of H.264. We achieved a 129:1 compression ratio if a lossless encoding is used, and Fig. 5(a) shows the result. If we encode the video at various lossy levels, placing the color texture in a mosaic fashion to the right of the RGB encoded image, we can achieve even higher compression ratios. For example, we achieved a 551:1 compression ratio if the video frames are compressed using 4:2:0 subsampling and a constant rate factor (CRF) of 6. Figure 5(b) shows the representative result using this level of lossy compression; it only requires a 14 Mbps connection to stream live 3D video at this quality. If lower quality geometry is acceptable, we achieved a 1,602:1 compression ratio using a CRF value of 12 to encode the video sequence. It would only require a 4.8 Mbps network connection to stream this quality video at 30 Hz. As shown in Fig. 5(c), even at the very low bitrate of 4.8 Mbps the resulting 3D reconstructions are still of high quality in both geometry and color texture. The mean error between the original and reconstructed geometries across was 0.38 mm, 0.65 mm, and 0.69 mm for CRF values of 0, 6, and 12, respectively. The respective standard deviations were 0.50 mm, 0.51 mm, and 0.54 mm. It should be noted that these measurements excluded large boundary outliers.

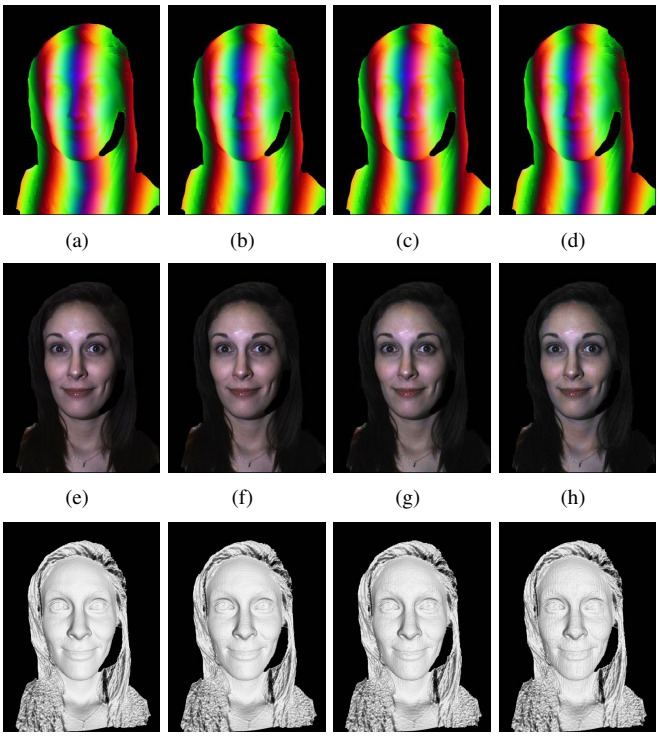

(a) (b) (c) (d)

(e) (f) (g) (h)

(i) (j) (k) (l)

Fig. 4. Compressing encoded RGB images with lossy JPEG encoding at different qualities. (a) - (d) JPEG quality of 100%, , 95%, 90%, and 85%, respectively; (e) - (h) recovered texture from RGB images (a)-(d), respectively; (i)-(l) recovered 3D geometry from RGB images (a)-(d), respectively.

C. Holostream

As a result of the above process, the encoded 3D video is small enough for delivery across wired or wireless networks. To demonstrate this, we implemented data transmission within an intermediary web server—built on top of HTTP and WebSocket technologies. When a client first connects to the server, an initialization message is constructed and sent over a WebSocket. This message contains a few important parameters, such as the camera's demosaicing format and resolution, the encoding parameters, etc. After initialization, encoded live video streams are delivered over HTTP to connected clients within small video segments (transport streams) via HTTP Live Streaming (HLS). On the receiving end, the compressed video received can be decompressed, and the decompressed 2D video can be used frame-by-frame to reconstruct 3D geometry and color texture.

We then developed a complete demonstration system to verify the performance of our proposed 3D video sensing and streaming methods. The entire system was implemented with a single 3D video sensing system on a single PC. The PC has an Intel Core i7 (3.40 GHz) CPU, 16 GB of RAM, and a single NVIDIA GeForce GTX 980 Ti GPU. The real-time 3D video sensing system consisted of a single camera (PointGrey

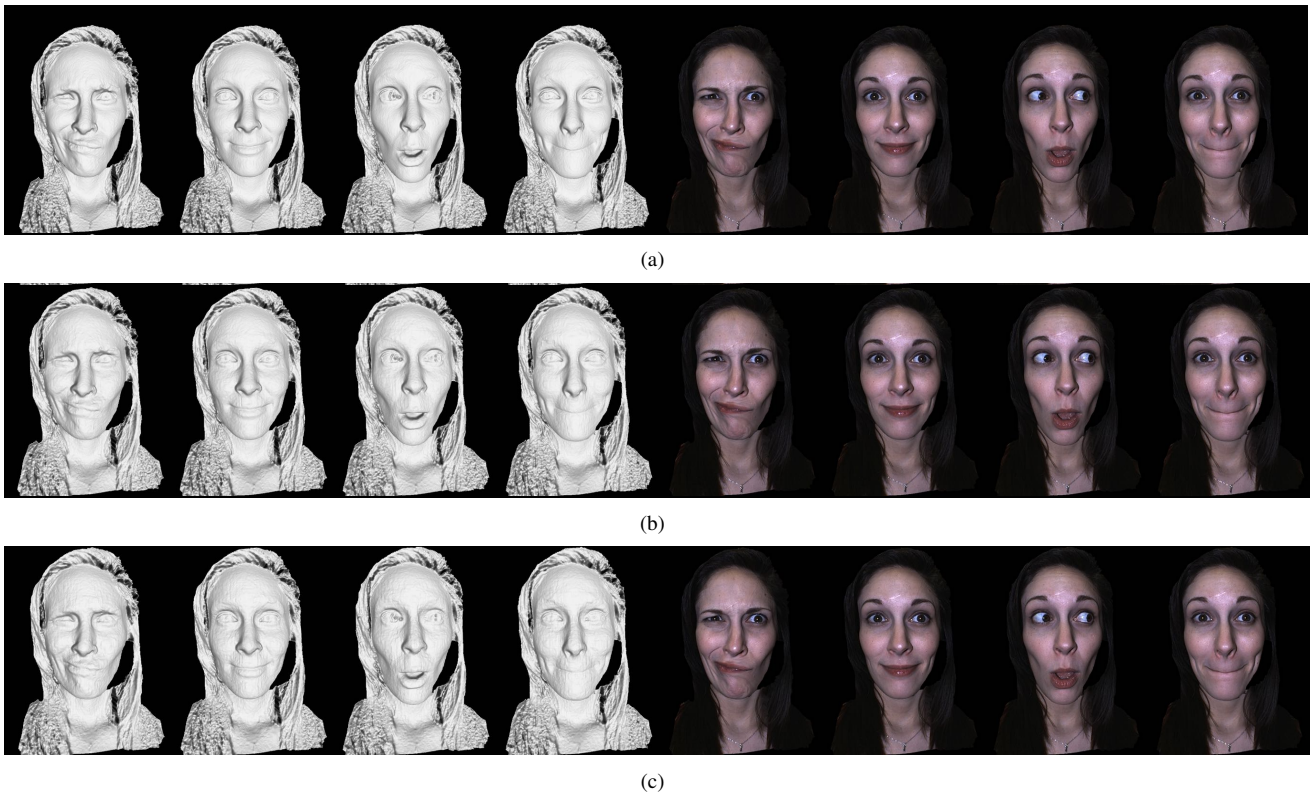

Fig. 5. Compressing RGB image sequences with H.264 video encoding. (a) Four frames decoded from encoded video stored with lossless H.264 (129:1 compression ratio); (b) four frames decoded from video stored with lossy H.264 using a CRF of 6 (551:1 compression ratio); (c) four frames decoded from video stored with lossy H.264 using a CRF of 12 (1,602:1 compression ratio). The left half of (a)-(c) shows the recovered 3D data in shaded mode; the right half shows the recovered color texture mapped onto the recovered 3D data.

Grasshopper3 GS3-U3-23S6C) and a single DLP projector (Texas Instruments LightCrafter 4500); the resolution of the camera was chosen as 480 $\times$ 640 and the projector's resolution was 912 $\times$ 1140.

Our real-time 3D optical sensing technique requires six fringe patterns to reconstruct one single 3D geometry frame. For the high frequency patterns, a fringe period $T_1 = 36$ pixels was used; for the lower frequency fringe patterns, a period of $T_2 = 380$ pixels was used. To achieve a sensing rate of at least 30 Hz, we project and capture images at 180 Hz. We implemented the method developed by Zhang and Huang [27] to calibrate our 3D optical sensing system, providing measurement accuracies between 0.1-0.2 mm.

The entire sensing and compression framework was implemented on the GPU within custom CUDA kernels in order to maintain a streamable frame rate of at least 30 (3D) Hz. Figure 6 shows two photographs of the implementation of our Holostream platform. Figure 6(a) shows the system that includes real-time 3D optical sensing, 3D video compression, and 3D video streaming. As mentioned above, all of the video data processing was carried out on a single PC. Figure 6(b) shows multiple users visualizing the 3D video being delivered to their mobile devices across the standard wireless network on Purdue University's campus.

III. CONCLUSIONS

This paper presented both 3D video optical sensing and streaming technologies. This platform enabled high-quality 3D video delivery across standard wireless networks, even to mobile devices (e.g., iPhones, iPads). The 3D video compression method achieved compression ratios of 1,602:1 while maintaining high quality when paired with the H.264 codec. The prototype system we developed demonstrated the entire 3D optical sensing acquisition, encoding, compression, decompression, and visualization framework. This system wirelessly delivered coordinate and color data, consisting of up to 307,200 vertices per frame, at 30 Hz to multiple mobile phones and tablets. Such a platform technology could find many applications within the mechatronics community, especially when remote sensing and remote operation are of interest.

REFERENCES

[1] T. Bell, J. Allebach, and S. Zhang, "Holostream: High-accuracy, high-speed 3d range video," ser. IS&T International Conference on Electronic Imaging, Burlingame, California, 2018.

[2] T. Bell, B. Vlahov, J. P. Allebach, and S. Zhang, "Three-dimensional range geometry compression via phase encoding," *Appl. Opt.*, vol. 56, no. 33, pp. 9285–9292, 2017.

[3] T. Bell and S. Zhang, "Multi-wavelength depth encoding method for 3d range geometry compression," *Appl. Opt.*, vol. 54, no. 36, pp. 10 684–10 961, 2015.

(a)

(b)

Fig. 6. Real-time 3D optical sensing and streaming system. (a) Real-time 3D optical sensing, compression, and streaming system; (b) real-time 3D video visualization on mobile devices of the video delivered across a standard wireless network on Purdue University's campus.

[4] X. Chen and S. Zhang, "Three-dimensional range geometry and texture data compression with space-filling curves," *Opt. Express*, vol. 25, no. 21, pp. 26 148–26 159, 2017.

[5] U. R. Dhond and J. K. Aggarwal, "Structure from stereo-a review," *IEEE Trans. Systems, Man. and Cybernetics*, vol. 19, no. 6, pp. 1489–1510, 1989.

[6] D. C. Ghiglia and M. D. Pritt, Eds., *Two-Dimensional Phase Unwrapping: Theory, Algorithms, and Software*. New York: John Wiley and Sons, 1998.

[7] M. Hansard, S. Lee, O. Choi, and R. P. Horaud, *Time-of-Flight Cameras*. Springer-Verlag London, 2013.

[8] Y. Huang, Y. Shang, Y. Liu, and H. Bao, *Handbook of 3D Machine Vision: Optical Metrology and Imaging*, 1st ed. CRC, 2013, ch. 3D shapes from Speckle, pp. 33–56.

[9] J.-S. Hyun and S. Zhang, "Enhanced two-frequency phase-shifting method," *Appl. Opt.*, vol. 55, no. 16, pp. 4395–4401, 2016.

[10] A. Jones, M. Lang, G. Fyffe, X. Yu, J. Busch, I. McDowall, M. Bolas, and P. Debevec, "Achieving eye contact in a one-to-many 3d video teleconferencing system," *ACM Trans. Graph.*, vol. 28, no. 3, pp. 64:1–64:8, 2009.

[11] N. Karpinsky and S. Zhang, "Composite phase-shifting algorithm for three-dimensional shape compression," *Opt. Eng.*, vol. 49, no. 6, p. 063604, 2010.

[12] ——, "3d range geometry video compression with the h.264 codec," *Opt. Laser Eng.*, vol. 51, no. 5, pp. 620–625, 2013.

[13] N. Lazaros, G. C. Sirakoulis, and A. Gasteratos, "Review of stereo vision algorithms: From software to hardware," *International Journal of Optomechatronics*, vol. 2, no. 4, pp. 435–462, 2008.

[14] B. Li, Y. An, D. Cappelleri, J. Xu, and S. Zhang, "High-accuracy, high-speed 3d structured light imaging techniques and potential applications to intelligent robotics," *Intl Journal of Intelligent Robotics and Applications*, vol. 1, no. 1, pp. 86–103, 2017.

[15] K. Liu, Y. Wang, D. L. Lau, Q. Hao, and L. G. Hassebrook, "Dual-frequency pattern scheme for high-speed 3-d shape measurement," *Opt. Express*, vol. 18, pp. 5229–5244, 2010.

[16] D. Malacara, Ed., *Optical Shop Testing*, 3rd ed. New York, NY: John Wiley and Sons, 2007.

[17] P. Ou and S. Zhang, "Natural method for three-dimensional range data compression," *Appl. Opt.*, vol. 52, no. 9, pp. 1857–1863, 2013.

[18] J. Pan, P. Huang, S. Zhang, and F.-P. Chiang, "Color n-ary gray code for 3-d shape measurement," in *12th International Conference on Experimental Mechanics*, Politecnico di Bari, Italy, 2004.

[19] J. Salvi, S. Fernandez, T. Pribanic, and X. Llado, "A state of the art in structured light patterns for surface profilometry," *Patt. Recogn.*, vol. 43, no. 8, pp. 2666–2680, 2010.

[20] T. Weise, B. Leibe, and L. V. Gool, "Fast 3d scanning with automatic motion compensation," in *IEEE Conference on Computer Vision and Pattern Recognition (CVPR)*, 2007, pp. 1–8.

[21] S. Zhang, "Recent progresses on real-time 3-d shape measurement using digital fringe projection techniques," *Opt. Laser Eng.*, vol. 48, no. 2, pp. 149–158, 2010.

[22] ——, "Three-dimensional range data compression using computer graphics rendering pipeline," *Appl. Opt.*, vol. 51, no. 18, pp. 4058–4064, 2012.

[23] ——, *High-speed 3D imaging with digital fringe projection technique*, 1st ed. New York, NY: CRC Press, 2016.

[24] ——, "Absolute phase retrieval methods for digital fringe projection profilometry: a review," *Opt. Laser Eng.*, vol. 107, pp. 28–37, 2018.

[25] ——, "High-speed 3d shape measurement with structured light methods: a review," *Opt. Laser Eng.*, vol. 106, pp. 119–131, 2018.

[26] S. Zhang and P. S. Huang, "High-resolution real-time three-dimensional shape measurement," *Opt. Eng.*, vol. 45, no. 12, p. 123601, 2006.

[27] ——, "Novel method for structured light system calibration," *Opt. Eng.*, vol. 45, no. 8, p. 083601, 2006.

[28] S. Zhang, D. Royer, and S.-T. Yau, "Gpu-assisted high-resolution, real-time 3-d shape measurement," *Opt. Express*, vol. 14, no. 20, pp. 9120–9129, 2006.